Appl. Phys. A 64, 451–455 (1997)

Applied Physics A Materials Science & Processing



# UV-laser-induced periodic surface structures on polyimide

**M. Himmelbauer, N. Arnold, N. Bityurin*, E. Arenholz, D. Bäuerle**

Angewandte Physik, Johannes-Kepler-Universität Linz, A-4040 Linz, Austria
(Fax: + 43-732/2468-9242)

Received: 14 November 1996/Accepted: 4 December 1996

**Abstract.** The formation of interference gratings generated by pulsed UV-laser irradiation of polyimide is discussed on the basis of recent experimental investigations on laser-induced surface topology changes. The model suggested permits one to interpret row doubling and to estimate both the range of fluences where periodic surface structures are formed and the ratio between the period and width. Formulas for the energy deposition in the interference arrangement and for the influence of heat diffusion are presented. This allows us to distinguish between thermal and non-thermal processes.

**PACS:** 42.60; 81.60

Laser-light irradiation of materials frequently results in the formation of coherent or non-coherent structures [1]. The period of coherent structures, $\Lambda$, depends on both the laser parameters and the physical properties of the material. The most well-known coherent structures of this type are the so-called ripples. In polymers, ripples originate from the interference between the incident laser light and the light scattered along the surface. Well-pronounced ripples are formed in only a small range of fluences, mainly below the threshold fluence for ablation, $\phi_{th}$, and with a large number of laser pulses, typically some $10^3$ [1–11]. Another type of coherent structures are large-area interference gratings, which are studied mainly with respect to applications in microelectronics [12–15]. Because high contrast is generated by interfering laser beams from the beginning of irradiation and ablation does not necessarily destroy the interference pattern, well-pronounced gratings can be fabricated by using, typically, some 10 pulses only. For the generation of both types of structures, mainly excimer lasers ($\lambda = 193$ and 248 nm; $\tau_l = 10$–40 ns) and harmonics of Nd:YAG lasers (4-th harmonic: $\lambda = 266$ nm; $\tau_l = 3$–5 ns) have been employed [5–15].

In this paper we suggest for the case of polyimide (Kapton H) an explanation for structure formation as observed in [13–15]. For subthreshold fluences these authors observed single raised ridges with no ablated valleys. The heights of the ridges were in the range of some 10 nm. For fluences well above $\phi_{th}$, ablated valleys were observed, and the raised ridges were split into double rows. The explanation is based on recent investigations of surface topology changes observed under pulsed UV-laser irradiation (center wavelength $\lambda_C = 302$ nm; 140 ns $\leq \tau_l \leq 5$ µs) [16, 17]. Here, three different features, which are schematically shown in Fig. 1, were found: swelling of the irradiated volume (hump formation), lowering of the irradiated area below the level of the untreated surface (dent formation), and real material removal (ablation) with hole formation. Ablation was tentatively interpreted on the basis of a thermal process and a (thermal or non-thermal) mechanism that diminishes the apparent activation energy for the desorption of species from the surface. Hump formation may be related to the amorphization (random coiling) of crystalline domains and to the (thermal or non-thermal) scission of polymer chains [16], or to non-elastic deformations caused by the gases produced within the irradiated volume. Dent formation may originate from plastic deformations caused by surface tension effects. Due to the small depth of dents, typically a few nm, this process will be subsequently ignored.

## 1 Structure formation

### *1.1 Interference gratings*

Interference gratings are periodic surface structures produced by the interference of two beams that are superimposed at the sample surface [1]. Let us consider two identical $\sigma$-polarized beams with angels of incidence $\Theta_i$, and with equal fluences, $\phi_0$ (measured perpendicularly to their direction of propagation). At the gas–solid interface, the average fluence normal to the surface is then $\phi_i = 2\phi_0 \cos\Theta_i$. The distribution of the fluence, defined as the $z$ component of the energy flux *below* the surface, is then given by

$$\phi(x,z) = A(\Theta_i)\phi_i\,(1 + V\cos kx)\exp(-\beta z)\,. \qquad (1)$$

Here, $A(\Theta_i) = 1 - R(\Theta_i)$ is the absorptivity of the material, and $V$ is the visibility of the interference pattern on the surface.

*On leave from: Institute of Applied Physics, Russian Academy of Sciences, 603600 Nizhnii Novgorod, Russia

$k$ is the wavevector of this pattern and

$$\beta = \frac{4\pi}{\lambda} \operatorname{Im}(\tilde{n}\cos\Theta_t)\,, \tag{2}$$

where $\lambda$ is the laser wavelength in vacuum, $\tilde{n}$ the complex index of refraction, and $\Theta_t$ the *complex* angle of refraction. If the substrate is a *weak* absorber, then $\beta \approx \alpha/\cos\Theta$, where $\alpha$ is the absorption coefficient and $\Theta$ is the real angle of refraction.

Let us consider first a photochemical process where the surface transformation is related to the deposited energy per unit volume.

The *energy absorbed* per unit volume is given by the derivative of (1) with respect to $z$. Near the surface $z = 0$ this yields

$$H(\Theta_i, x) = A(\Theta_i)\beta\phi_i(1 + V\cos kx)\,. \tag{3}$$

Alternatively, one can consider the deposited energy to be proportional to the square of the electric field and the imaginary part of the dielectric constant, and obtain:

$$A(\Theta_i)\beta = \frac{t_i\bar{t}_i}{\cos\Theta_i}\frac{2\pi}{\lambda}\operatorname{Im}(\tilde{\varepsilon})\,, \tag{4}$$

where $t_i$ is the *amplitude* transmission coefficient at the interface. The upper dash denotes complex conjugation.

Assume that at normal incidence a particular surface transformation takes place if $\phi \geq \phi_{th} \equiv \phi_{th}(\Theta_i = 0)$. At oblique incidence the transformation at point $x$ takes place if the energy deposited per unit volume near the surface is $H(\Theta_i, x) \geq H(0)$, where at the threshold the energy deposition is given by

$$H(0) \equiv H(\Theta_i = 0) = A(0)\alpha\phi_{th}\,. \tag{5}$$

From (3) and (5) we obtain the condition for the surface transformation at the point $x$:

$$\phi_{th} \equiv \phi_{th}(\Theta_i = 0) \leq B\phi_i(1 + V\cos kx)\,, \tag{6}$$

where $B$ can be derived with (2) and (4):

$$B = \frac{A(\Theta_i)\beta}{A(0)\alpha} \equiv \frac{A(\Theta_i)\operatorname{Im}(\tilde{n}\cos\Theta_t)}{A(0)\operatorname{Im}(\tilde{n})} = \frac{t_i\bar{t}_i}{t_n\bar{t}_n\cos\Theta_i}\,, \tag{7}$$

where $t_n$ is the transmission coefficient for normal incidence. $B$ depends on $\Theta_i$ and reflects the changes in energy deposition for oblique incidence with respect to normal incidence, if the fluences just *above the surface* are the same.

According to the surface topology changes exhibited in Fig. 1, we can distinguish two cases for which humps are formed. Here, we introduce $\phi_{hu} \equiv \phi(r_{hu})$, which is the fluence above the sample at $r = r_{hu}$ in single-beam experiments at normal incidence and $\phi_{max} \equiv B\phi_i(1 + V)$.

*Case (a)*: $\phi_{hu} \leq \phi_{max} < \phi_{th}$

Figure 2 shows the interference pattern (6) for $V < 1$ (dashed curves) together with the surface-topology changes expected from Fig. 1. In regions where the fluence of the interference pattern exceeds $\phi_{hu}$, the surface is elevated. The height of humps is some 10 nm [16]. With (6) the width of humps can be estimated from

$$w_{hu} = \frac{\Lambda}{\pi}\arccos\left(\frac{\frac{\phi_{hu}}{B\phi_i} - 1}{V}\right). \tag{8a}$$

The ratio $w_{hu}/\Lambda$ is plotted in Fig. 3 as a function of $\phi_i$, and with $\Theta_i = 48°$, $V = 0.9$, and $B = 0.933$ (dashed curve). Here, we employed $\phi_{hu} \approx 0.7\phi_{th}$, as found with $Ar^+$-laser radiation ($\lambda \approx 302$ nm) in [16]. $\phi_{th}$ was taken to be 52 mJ/cm$^2$ and $B$ was calculated from (7) with $\tilde{n} = 1.85 + 0.6i$ [18]. Note, that with the parameters employed the value of $B$ is close to unity, which was used in [14]. This explains why the value of $\phi_{th} = 55$ mJ/cm$^2$ found in [14] is in good agreement with the value employed in the present analysis.

*Case (5)*: $\phi_{max} \geq \phi_{th}$

For fluences of the interference pattern above $\phi_{th}$, ablation takes place, and it will lead to the profile shown in Fig. 1b. The widths of the holes, $w_{ho}$, can be calculated from:

$$w_{ho} = \frac{\Lambda}{\pi}\arccos\left(\frac{\frac{\phi_{th}}{B\phi_i} - 1}{V}\right). \tag{8b}$$

The ratio $w_{ho}/\Lambda$ as a function of $\phi_i$ is included in Fig. 3 by the full curve. Ablation will lead to hump splitting, as shown in Fig. 2b. If $\phi_{max}$ is further increased, neighboring humps will almost merge and form double rows (Fig. 2c). This can explain the experimental data in [14] which are in reasonable agreement with the full curve in Fig. 3. However, there exists a discrepancy between the value $\phi_{th} \approx 52$ mJ/cm$^2$, necessary to fit the data [14], and the value $\phi_{th}(\lambda = 248\text{ nm}) \approx 40$ mJ/cm$^2$ [19, 20] observed for normal

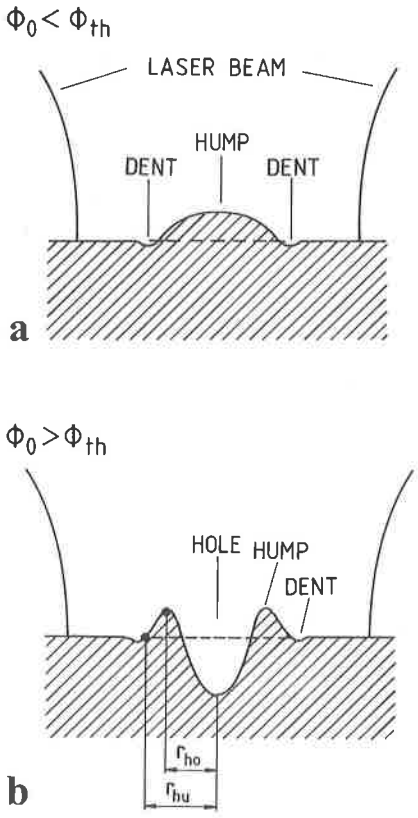


**Fig. 1a,b.** Schematic drawings of the surface topology observed on polyimide after focused single-shot UV-laser-beam irradiation with $\phi(r) = \phi_0\exp(-(r/w_0)^2)$ [16]. The dashed line indicates the initial polymer surface. **a** $\phi_0 < \phi_{th}$. **b** $\phi_0 > \phi_{th}$

incidence and single beam experiments. Let us show that this may indicate that pattern formation is mainly *thermal* in nature.

Consider a model, that relates surface transformations to the *temperature* induced in the specimen. The source term in the corresponding linear heat conduction problem can be written in analogy to (1) and (3) as

$$Q(x,y) = A(\Theta_i) I_i \beta (1 + V \cos kx) \exp(-\beta z) . \tag{9}$$

Here, $I_i$ is the average intensity of the two beams above the sample surface. The solution can be found by describing the overal temperature rise, $\Delta T$, by a uniform and an oscillating part $\propto \cos kx$ (see Appendix). With a rectangular laser pulse the solution at the surface $z = 0$ can be written as

$$\Delta T(x,t) = \frac{A(\Theta_i) I_i}{\beta \kappa} T_1(D\beta^2 t) \left[1 + V V_T(D\beta^2 t) \cos kx\right] . \tag{10}$$

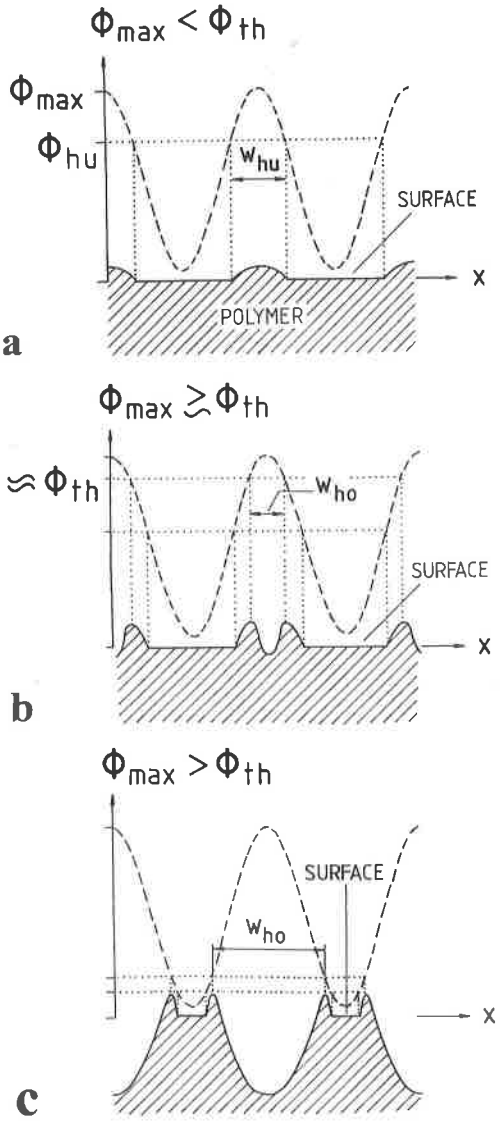


**Fig. 2a–c.** Schematic drawings of the interference pattern $\phi(x)$ with $V = 0.9$ and period $\Lambda$ (dashed curve) and the corresponding surface topology changes of the interference pattern. **a** $\phi_{max} < \phi_{th}$. **b** $\phi_{max} \gtrsim \phi_{th}$. **c** $\phi_{max} > \phi_{th}$

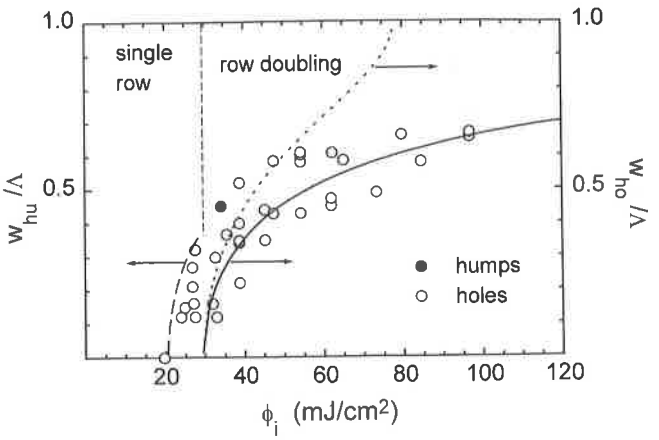


**Fig. 3.** Calculated width of humps $w_{hu}$ (dashed curve), and holes $w_{ho}$ (solid curve, dotted curve) of interference gratings normalized to $\lambda$, as a function of $\phi_i$. In all cases $B = 0.933$. Solid curve: $\phi_{th} = 52$ mJ/cm$^2$, $V = 0.9$. Dashed curve: $\phi_{hu} \approx 0.7$, $\phi_{th} \approx 36$ mJ/cm$^2$, $V = 0.9$. Dotted curve: $\phi_{th} = 40$ mJ/cm$^2$, $VV_T = 0.45$. The vertical dotted line marks the transition from single to double rows. The filled circle shows the width of a raised ridge. The experimental data (open circles, filled circle) are taken from [14, 15]

Here, $\kappa$ is the thermal conductivity, $D$ is the heat diffusivity, $T_1(t^*)$ is a dimensionless surface temperature rise for finite absorption, and $t^* \equiv D\beta^2 t$ is a dimensionless time. $T_1(t^*)$ is given by

$$T_1(t^*) = \frac{2}{\sqrt{\pi}} t^{*1/2} + \exp(t^*) \operatorname{erfc}(t^{*1/2}) - 1 . \tag{11}$$

$V_T$ in (10) is the decrease in visibility caused by heat diffusion. In other words, $V_T$ accounts for the fact that the "visibility" of the temperature distribution is smaller than that of the energy deposition. $V_T$ is given by (see Appendix)

$$V_T(t^*) = \exp(-qt^*) + \frac{q}{T_1(t^*)} \int_0^{t^*} \exp(-q\tau) T_1(\tau)\, d\tau , \tag{12}$$

or, in the general case of a time-dependent pulse shape, characterized by the temporal intensity profile $I(t^*)$:

$$V_T'(t^*) = \frac{\int_0^{t^*} I(t^* - \tau) \exp(-q\tau) \frac{dT_1(\tau)}{d\tau}\, d\tau}{\int_0^{t^*} I(t^* - \tau) \frac{dT_1(\tau)}{d\tau}\, d\tau} \tag{12a}$$

with

$$q = k^2/\beta^2 \equiv (2\pi l_\beta/\Lambda)^2 . \tag{13}$$

$V_T$ monotonously decreases with time, from $V_T(0) = 1$ to $V_T(\infty) = 0$. The typical dependence $V_T'(t^*)$, together with the intensity and the temperature rise, normalized to their maximum values, are shown in Fig. 4.

From (10) it is clear that heat diffusion decreases the overall visibility for a thermal process, and thus increases the threshold fluence. For mainly thermally induced surface transformations we can rewrite (6) in the form

$$\phi_{th\,T} \le B_T \phi_i \left(1 + V V_T(D\beta^2 \tau_1) \cos kx\right) \tag{14}$$

with

$$B_T = B \frac{\alpha^2}{\beta^2} \frac{T_1(D\beta^2 \tau_1)}{T_1(D\alpha^2 \tau_1)} . \tag{15}$$

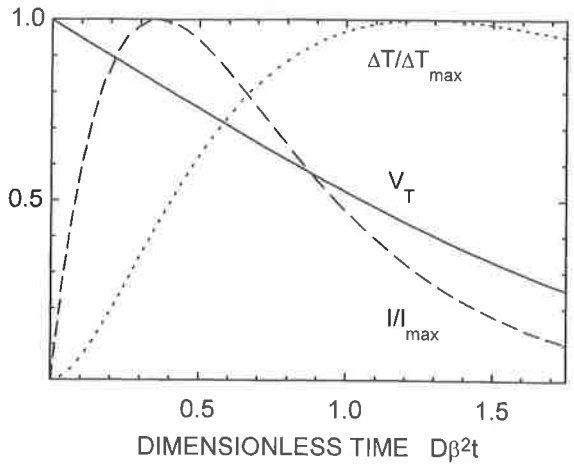


**Fig. 4.** Calculated dependence of visibility $V_T'(t^*)$ (solid curve) together with the intensity $I(t) \propto (t/\tau_l)\exp[-(t/\tau_l)+1]$ ($\tau_l = 10$ ns [21], dashed curve), and the corresponding surface temperature rise (dotted curve), normalized by their maximum values. For normalization of the time $t^*$ we have employed $(D\beta^2)^{-1} \approx 25$ ns

For the derivation of (14) we used (10) and the relation between the threshold fluence for normal incidence and the threshold temperature rise

$$\Delta T_{th} = \frac{A(0)\phi_{th\,T}}{\alpha\kappa\tau_l} T_l(D\alpha^2\tau_l). \tag{16}$$

The width of the ablated valleys follows from (14) in the same way as (8b) follows from (6).

$$w_{ho} = \frac{\Lambda}{\pi}\arccos\left(\frac{\frac{\phi_{th\,T}}{B_T\phi_i}-1}{VV_T}\right). \tag{8c}$$

Note that (8c) which describes the thermal process is similar to (8b). The main difference is that $B$ has been substituted by $B_T$, and $V$ by $VV_T$. As a consequence the optimal fit to the data in Fig. 3 yields a value of $\phi_{th\,T}$ which differs from $\phi_{th}$.

The threshold fluence for surface transformations in the interference arrangement, $\phi_{th}(\Theta_i)$, can be determined experimentally. For transformations based on *energy deposition* it is related to the $\phi_{th}(\Theta_i = 0)$ via

$$\phi_{th}(\Theta_i = 0) = B\phi_{th}(\Theta_i)(1+V). \tag{17}$$

If the transformation occurs above a certain *temperature*, the threshold $\phi_{th}(\Theta_i)$ corresponds to a threshold $\phi_{th\,T}(\Theta_i = 0) < \phi_{th}(\Theta_i = 0)$. The relation between $\phi_{th}(\Theta_i)$ and $\phi_{th\,T}(\Theta_i = 0)$ follows from (14)

$$\phi_{th\,T}(\Theta_i = 0) = B_T\phi_{th}(\Theta_i)\left[1+VV_T(D\beta^2\tau_l)\right]. \tag{18}$$

Equations (17) and (18) allow one to elucidate the underlying mechanisms by changing the angle of incidence, $\Theta_i$, or the laser pulse duration $\tau_l$. The ratio of the threshold values calculated from (17) and (18) for the same experimentally measured $\phi_{th}(\Theta_i)$ is

$$\frac{\phi_{th\,T}(\Theta_i = 0)}{\phi_{th}(\Theta_i = 0)} = \frac{B\left[1+VV_T(D\beta^2\tau_l)\right]}{B(1+V)}. \tag{19}$$

With the numbers employed for $\Theta_i = 48°$, $\alpha \approx \beta$ and consequently $B \approx B_T$. Thus, the main difference arises from the change in the overall visibility. With $V = 0.9$, $D = 0.45 \times 10^{-3}$ cm$^2$/s, $\tau_l = 30$ ns, and $\beta \approx \alpha = 3 \times 10^5$ cm$^{-1}$, the value of $V_T$ calculated from (12) is $V_T \approx 0.5$, and we obtain $\phi_{th\,T}(\Theta_i = 0) = 0.76\phi_{th}(\Theta_i = 0)$ [a similar value of $V_T$ is obtained for the time-dependent intensity at the moment when the maximum temperature is reached (see Fig. 4)]. Thus, heat diffusion significantly decreases the effective visibility $VV_T$ which is essential for processes that are governed by the temperature. This may explain the differences between the threshold fluences $\phi_{th} = 40$ mJ/cm$^2$ and $\phi_{th} = 52$ mJ/cm$^2$. The first value was measured in a single-beam experiment at normal incidence. The value $\phi_{th} = 52$ mJ/cm$^2$ was derived by fitting the experimental data obtained in the interference experiments (Fig. 3) by the (photochemical) Eq. (8b). For a *thermal* process the data should be fitted by formula (8c) which yields a smaller value of $\phi_{th}$. Heat diffusion will *lower the overall visibility* for all fluences. A good fit to the experimental data in Fig. 3 *at low* fluences can be provided by using (8c), with the overall visibility $VV_T \approx 0.45$, $B_T = 0.933$ and $\phi_{th} = 40$ mJ/cm$^2$ (dotted curve). At higher fluences however, significant differences between the data and the dotted curve are revealed. The reason for this discrepancy may be related to the ablation process itself. When ablation takes place within the valleys, it requires additional energy. As a result, the temperature near the edges of the valleys decreases. Correspondingly, the width of the ablated valleys becomes smaller than that calculated from (10). The hump width in Fig. 3 recalculated on the basis of a thermal model (14) practically coincides with the dashed curve in the region of low fluences where the hump exists. The filled circle shows the width of a raised ridge taken from [15]. The absence of systematic investigations into the width of ridges does not allow a detailed comparison of the dashed curve with the experimental results.

### *1.2 Ripples*

The formation of ripples is based on the interference of a (single) incident laser beam and the light scattered within the surface [1]. With insulators, the scattered intensity is small compared to the incident intensity, so that $\phi_s \ll \phi_i$. Thus, the interference pattern is mainly determined by $\phi_i$. It has a much smaller visibility, and the fluence on the surface can be described, in the simplest approximation, by $\phi(x) \approx C(\Theta_i)\phi_i[1+2\gamma(\phi_s/\phi_i)^{1/2}\cos(k_r x)]$ where $k_r = 2\pi/\Lambda_r$. $\gamma < 1$ describes the mutual coherence and polarization differences between the incident and scattered light. $C(\Theta_i)$ is of the order of unity, and $\Lambda_r$ depends on the wavelength and the angle of incidence of the laser light and on the material properties. Ripples are formed within a certain range of fluences $\phi_l \le \phi_{max} \le \phi_{th}$. The upper limit is determined by ablation which destroys the interference pattern. The lower limit, $\phi_l$, may again be related to hump formation. However, with the laser fluences employed for ripple formation (8 mJ/cm$^2 \lesssim \phi_i \lesssim 11$ mJ/cm$^2$ [22]), it becomes evident that this mechanism can not form ripples in a single-shot experiment, because even in the maxima of the interference pattern, the intensity is much lower than required for hump formation (about $0.7\phi_{th} \approx 30$ mJ/cm$^2$, as derived from the experiments [16]). On the other hand, the fluence for hump

formation in multiple-shot experiments can be lower, due to a laser-induced increase in absorption, an accumulation of the ripple profile, etc. Ripple formation due to multiple-shot laser irradiation may be initiated also by the depression of the surface originating from the slow elimination of small fragments produced within the bulk of the material. Thermodegradation of PI is more effective in the presence of oxygen [23]. The small fragments leave the surface by diffusion. This may result in a decrease in the thickness due to free volume relaxation, as observed for multiple-pulse irradiation of PI [24]. Another reason for such a depression can be thermal etching of PI in the presence of oxygen, as reported for millisecond $Ar^+$-laser pulses [25].

## 2 Conclusion

Interference gratings generated on polyimide by pulsed UV-laser radiation can be interpreted via surface topology changes previously observed in single-shot experiments. Interference gratings are formed if the maximum fluence of the interference pattern exceeds the fluence for hump formation. With fluences $\phi_{max} > \phi_{th}$, ablation in the center of the humps can cause row doubling. Analytical formulas for the energy deposition and the temperature distribution in the interference arrangement are provided. By comparing the threshold conditions for irradiation at normal incidence and for the oblique two-beam interference arrangement, additional information on the mechanisms mainly responsible for structure formation can be obtained.

*Acknowledgements.* We wish to thank the "Fonds zu Förderung der Wissenschaftlichen Forschung in Österreich" for financial support.

## Appendix

Let us consider the heat equation

$$T_t = D(T_{xx}+T_{zz})+\frac{Q}{c\varrho}. \tag{A.1}$$

Here, indices denote the corresponding derivatives. The source term $Q$ is given by (9). If the temperature is referred to the background value, the boundary and initial conditions are:

$$T_z(z=0)=0, \qquad T(z=\infty)=0, \qquad T(t=0)=0. \tag{A.2}$$

We search for a solution of (A.1)–(A.2) in the form

$$T(x,z,t) = T_a(z,t)+T_v(z,t)\cos kx. \tag{A.3}$$

Then, for both $T_a$ and $T_v$, the conditions (A.2) should hold, and $T_a$ and $T_v$ satisfy the equations

$$T_{a,t} = DT_{a,zz}+\frac{Q_a}{c\varrho} \tag{A.4a}$$

$$T_{v,t} = DT_{v,zz}-Dk^2T_v+\frac{VQ_a}{c\varrho}. \tag{A.4b}$$

Here, $Q_a$ is the spatially homogeneous part of (9). With the substitution $T_v = \tilde{T}_v\exp(-Dk^2t)$ one obtains

$$\tilde{T}_{v,t} = D\tilde{T}_{v,zz}+\exp(Dk^2t)V\frac{Q_a}{c\varrho} \tag{A.5}$$

Both (A.4a) and (A.5) are one-dimensional time-dependent heat equations. Their solutions can be written in terms of the solution $\tilde{T}_l(z,t)$ for finite absorption $\beta$ and *unit* intensity. $T_a$ can directly be expressed via $\tilde{T}_l$:

$$T_a = A(\Theta_i)I_i\tilde{T}_l(z,t). \tag{A.6}$$

For the time-dependent source term in (A.5) $\tilde{T}_v$ can be obtained from $\tilde{T}_l$ by using Duhamel's formula:

$$\tilde{T}_v = VA(\Theta_i)I_i\int_0^t \exp(Dk^2t')\frac{\partial}{\partial t}\tilde{T}_l(z,t-t')\,dt'. \tag{A.7}$$

We express $T_v$ via $T_v$ given by (A.7), introduce $\tau = t-t'$, and integrate the result. Subsequently, we combine $T_a$ and $T_v$ according to (A.3) and introduce $t^* \equiv D\beta^2t$. This yields (10) to (12).

## References


1. D. Bäuerle: *Laser Processing and Chemistry* (Springer, Heidelberg 1996)
2. A.E. Siegmann, P.M. Fauchet: IEEE J. Quantum Electron. QE **22**, 1384 (1986)
3. A. Barborica, I.N. Mihailescu, V.S. Teodorescu: Phys. Rev. B **49**, 8385 (1994)
4. S.A. Akhmanov, V.I. Emel'yanov, N.I. Koroteev, V.N. Seminogov: Sov. Phys. Usp. **28**, 1084 (1985)
5. M. Sendova, H. Hiraoka: Jpn. J. Appl. Phys. **32**, 6182 (1993)
6. H. Hiraoka, M. Sendova, C.H. Lee: Jpn. J. Appl. Phys. **33**, 7135 (1994)
7. M. Bolle, S. Lazare: Appl. Surf Sci. **65/66**, 349 (1993)
8. M. Bolle, S. Lazare: Appl. Surf Sci. **69**, 31 (1993)
9. M. Bolle, S. Lazare: J. Appl. Phys. **73**, 3516 (1993)
10. P.E. Dyer, R.J. Farley: Appl. Phys. Lett. **57**, 765 (1990)
11. P.E. Dyer, R.J. Farley: J. Appl. Phys. **74**, 1442 (1993)
12. K.J. Jlcisin, R. Fedosejevs: Appl. Opt. **26**, 396 (1987)
13. H.M. Phillips, D.L. Callahan, R. Sauerbrey: Appl. Phys. Lett. **58**, 2761 (1991)
14. H.M. Phillips, D.L. Callahan, R. Sauerbrey, G. Szabo, Z. Bor: Appl. Phys. A **54**, 158 (1992)
15. H.M. Phillips, R. Sauerbrey: Opt. Engineering **32**, 2424 (1993)
16. M. Himmelbauer, E. Arenholz, D. Bäuerle, K. Schilcher: Appl. Phys. A **63**, 337 (1996)
17. M. Himmelbauer, E. Arenholz, D. Bäuerle: Appl. Phys. A **63**, 87 (1996)
18. E.T. Arakawa, M.W. Williams, I.C. Ashley, L.R. Painter: J. Appl. Phys. **52**, 3579 (1981)
19. R. Braun, R. Nowak, P. Hess, H. Oetzmann, C. Schmidt: Appl. Surf. Sci. **43**, 352 (1989)
20. T. Kefer: master thesis (Linz 1991)
21. R. Sauerbrey: private communication
22. E. Arenholz, J. Heitz, M. Himmelbauer, D. Bäuerle: ALT'95, SPIE Proc. (1996)
23. H.J. Düssel, H. Rosen, D.O. Hummel: Macromol. Chem. **177**, 2343 (1976)
    W.W. Wright: In *Developments in Polymer Degradation-3*, ed. by N. Grassie (Applied Science Publisher LTD, London 1981) p.1
24. A.P. Alexandrov, A.A. Babin, N. Bityurin, N.G. Bronnikova, S.V. Muraviov, L.V. Soustov, F.I. Feldshtein, ICONO'95, SPIE Proc.
25. R. Srinivasan, R.R. Hall, W.D. Loehle, W.D. Wilson, D.C. Allbee: J. Appl. Phys. **78**, 4881 (1995)